Modified Modular Multilevel Converter With Third-Order Harmonic Voltage Injection to Reduce Submodule Capacitor Voltage Ripples

Ming Huang, Zhen Kang, *Member, IEEE*, Weilin Li, *Member, IEEE*, Jianlong Zou, Xikui Ma, and Jianhua Li

***Abstract*—This article presents a modified modular multilevel converter (MMC) equipped with the middle-cells and control algorithm for medium voltage applications. It is intended to reduce the submodule (SM) capacitor voltage ripples by the third-order harmonic voltage injection (THVI) and second-order harmonic current injection (SHCI) without the common-mode voltage injected on the ac-side. On the one hand, using the proposed algorithm, the independent power degrees of freedom can be produced to eliminate the dominant fundamental part in arm powers, which can dramatically reduce the SM capacitor voltage ripples. On the other hand, the smaller amplitude of the SHCI can be obtained, which decreases the power losses. Meanwhile, by properly controlling the proposed middle-cells of the modified MMC, the compensated parts can be produced to eliminate the common-mode voltages caused by the THVI. Additionally, the arm power analysis of the modified MMC under different power factors is conducted, and the obtained results are discussed. The mathematical models of the SM capacitor voltages for the half-bridge based SMs and the proposed middle-cells in the modified MMC are also analyzed. Finally, the effectiveness of the theoretical analysis of the modified MMC is verified by simulation and experimental results.**

***Index Terms*—Capacitor voltage ripple, middle-cell, modular multilevel converter (MMC), second-order harmonic current injection (SHCI), third-order harmonic voltage injection (THVI).**

I. Introduction

THE modular multilevel converter (MMC) is one of the most competitive topologies for medium to high voltage applications due to its modular nature, low power losses, small voltage step and redundancy nature [1]–[4]. Compared to the cascaded H-bridge multilevel converters, the MMC system is free of the bulky transformer feeding the submodule (SM) dc sources. In the MMC system, the dc bus voltage and ac output voltage are composed of the floating SM capacitor voltages that can be easily balanced by absorbing compensated active powers from arm currents. For years of development, attention has been mostly paid on the circulating current suppressing method [5]–[7], balancing control [8]–[10], power quality improvement [11], and system efficiency [12]–[14]. Therefore, the MMC has become a promising scheme for medium to high voltage applications.

In the MMC system, the SM capacitors serve as medium platforms for exchanging powers between the input and output sides. However, the power exchange between the dc and ac sides usually results in an undesirable SM capacitor voltage ripple. Meanwhile, the existing research works have verified that the smaller SM capacitor voltage ripple would be in favor of reducing the size and weight of the SM capacitors, which occupy more than half of the overall size and weight of the MMC system. In [5], it has been demonstrated that the SM capacitor voltage ripple in the MMC system is mainly influenced by two factors: the common-mode power and the differential mode power in MMC. Theoretically, the influence of the common-mode power on the SM capacitor voltage ripple can be eliminated by transferring it to the dc side, which is at the expense of drawing undesirable second-order harmonics in circulating currents [15]. Generally, the SM capacitor voltage ripple is mostly influenced by the differential-mode power. Although the SM capacitor voltage ripple in the MMC can be extremely reduced by inserting high frequency voltages and currents into the phase legs, an unexpected large current ripple would introduce significant power losses [16]. Meanwhile, the inserted high frequency voltage in the MMC system can decrease the available modulation index range of the output voltages [16]–[20]. In addition, the undesirable common-mode voltages produced by the injected voltages are exposed on the ac side, which can harm the medium voltage motor windings during a long-term operation [17]. Although many novel MMC topologies have been proposed to eliminate the drawbacks caused by the high frequency harmonic injection [18]–[20], this mostly addresses the common-mode voltage problem, while the problems of large arm current ripple caused by the injected high frequency current and reduced modulation index range still exist.

Manuscript received March 31, 2020; revised June 15, 2020, August 9, 2020, and September 25, 2020; accepted October 28, 2020. Date of publication November 2, 2020; date of current version February 5, 2021. This work was supported in part by the Fundamental Research Funds for the Central Universities of China under Grants G2019KY05306 and G2020KY05106, and in part by the National Nature Science Foundation of China under Grant 51777169. *(Corresponding author: Zhen Kang.)*

Ming Huang, Zhen Kang, and Weilin Li are with the Department of Electrical Engineering, School of Automation, Northwestern Polytechnical University, Xi'an 710054, China (e-mail: minghuang@nwpu.edu.cn; kangzhen@nwpu.edu.cn; liweilin907@126.com).

Jianlong Zou and Xikui Ma are with the State Key Laboratory of Electrical Insulation and Power Equipment, School of Electrical Engineering, Xi'an Jiaotong University, Xi'an 710049, China (e-mail: superzou@mail.xjtu.edu.cn; maxikui@mail.xjtu.edu.cn).

Jianhua Li is with the State Grid Xian Electric Power Supply Company, Xi'an 710032, China (e-mail: jianhuali126@126.com).

Color versions of one or more of the figures in this article are available online at https://ieeexplore.ieee.org.

Digital Object Identifier 10.1109/TPEL.2020.3035286

Therefore, considering the severe power loss and reduced modulation index range caused by the high frequency harmonic injection, the third-order harmonic voltage injection (THVI) without injecting currents is preferred for the MMC system [21]–[26]. The THVI aims to redistribute the arm powers with faster flow powers between the upper and lower arms in the controllable range without increasing the rms value of the arm current. The existing research showed that the increased modulation index would result in the decreased amplitude of the fundamental part of the SM capacitor voltage ripple. Therefore, the related studies have been focused on pulling down the peak value of the arm reference for enlarging the available modulation index range [23], [24]. A detailed analysis of how the THVI influences the operating region of the MMC system is presented in [23]. In [24], an optimal THVI was proposed to calculate the magnitude and phase of the THVI online to increase the dc-link voltage utilization. Also, it was found that the peak value of the arm reference voltage changed with different power factors. Especially, in order to eliminate the undesirable fundamental frequency part in the SM capacitor voltage ripple, the MMC system should operate at the modulation index of 1.414, which is not feasible in the HBSM-based MMC system [25], [26]. Therefore, by adopting the THVI, the dominant fundamental part in the SM capacitor voltage ripple can be suppressed only in part in the HBSM based MMC, thus achieving only a limited reduction of the SM capacitor voltage ripple.

Aiming to reduce the SM capacitor voltage ripple by the THVI and second-order harmonic current injection (SHCI), this article introduces a modified MMC equipped with the middle-cells, which can suppress the common-mode voltages caused by the THVI in ac side. On the one hand, the proposed control strategy in the modified MMC provides the independent power degrees of freedom for the arm powers, which aims to eliminate the dominant fundamental part in the SM capacitor voltage ripple. On the other hand, by properly controlling the proposed middle-cells with specified switching states, the compensated voltages produced by the proposed middle-cells can suppress the undesirable common-mode voltages caused by the THVI. Theoretically, the proposed middle-cells in the modified MMC, acting as harmonic generators, can achieve any required ac voltages under sufficient switching frequency.

The rest of this article is organized as follows. Section II gives the detailed analysis and model of the modified MMC. In Section III, the influence of the THVI on the arm powers and SM capacitor voltages in the modified MMC are discussed, and the control strategy for the proposed middle-cells are also provided. In order to verify the effectiveness of the theoretical analysis of the modified MMC, the simulation and experimental results are presented in Section VI and Section V, respectively. Finally, Section VI concludes this article.

II. Analysis of the Modified MMC System

A. Basic Structure and Model of Modified MMC

The basic structure of the modified MMC is illustrated in Fig. 1, where it can be seen that it consists of three phases: phase *a*, *b*, and *c*. Each phase is equipped with the upper arm, lower arm, and proposed middle cell. The arms of a single phase in the modified MMC consist of *n* SMs and an inductor *L*. The basic structure of the SM is displayed in Fig. 2(a), where it can be seen that each SM consists of a capacitor and two power switches. Normally, the SM capacitor voltage is chopped by the two power switches, and the driven pulses of the power switches are controlled to have complementary features. Meanwhile, the inductors of phases mainly aim to avoid inrush currents caused by the SM switching pulses for reliability.

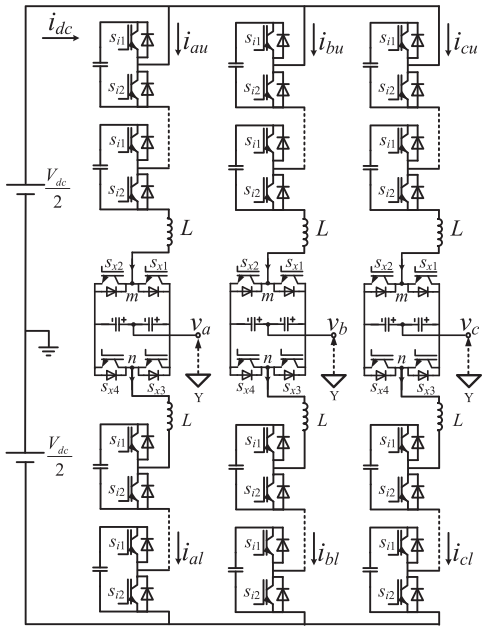

Fig. 1. Schematic structure of the modified MMC.

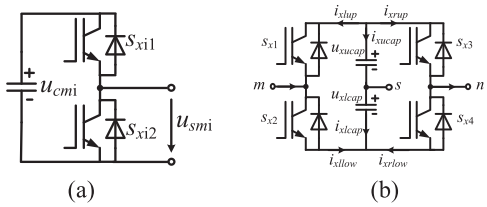

Fig. 2. SM structure of the modified MMC. (a) Half-bridge-based SM. (b) Proposed middle cell.

The basic structure of the proposed middle-cell is presented in Fig. 2(b). Unlike the SMs depicted in Fig. 2(a), the proposed middle-cell has three output terminals, denoted as *m*, *n*, and *s*, which are used to connect the upper arm, lower arm and ac side. Thus, the proposed middle-cell can be divided into three parts: the left arm, the right arm and the capacitor arm. The left and right arms consist of two power switches, and the capacitor arm includes two capacitors connected in series. Also, the switching pules of the power switches in the left and right arms of the proposed middle-cells are forced to be switched complementarily.

As shown in Fig. 2(b), the terminal voltages are produced by chopping the capacitor voltages with the power switches of the proposed middle-cells. It should be noted that the positive and negative voltages in u_{xms} are derived from the upper and lower

TABLE I
SWITCHING STATES OF THE PROPOSED MIDDLE-CELL

Switching States	u_{xms}	u_{xsn}	u_{xmn}
S_{x1}, S_{x3} are on, S_{x2}, S_{x4} are off	u_{xucap}	-u_{xucap}	0
S_{x1}, $S_{x3}$are off, S_{x2}, S_{x4} are on	-u_{xlcap}	u_{xlcap}	0
S_{x1}, S_{x4} are on, S_{x2}, $S_{x3}$are off	u_{xucap}	u_{xlcap}	u_{xucap}+u_{xlcap}
S_{x1}, S_{x4} are off, S_{x2}, S_{x3} are on	-u_{xlcap}	-u_{xucap}	-u_{xucap}-u_{xlcap}

capacitor voltages of the proposed middle-cell, respectively, while the positive and negative voltages in u_{xsn} are derived from the lower and upper capacitor voltages of the proposed middle-cell, respectively. Therefore, the terminal voltages of the middle-cells in the modified MMC can be expressed as

$$\begin{cases} u_{\mathrm{xms}} = s_{x1}u_{xucap} - s_{x2}u_{xlcap} \\ u_{\mathrm{xsn}} = -s_{x3}u_{xucap} + s_{x4}u_{xlcap} \end{cases} \tag{1}$$

where u_{xucap} and u_{xlcap} denote the upper and lower capacitor voltages in the middle-cell of phase x ($x = a, b, c$), respectively, and s_{xi} ($x = a, b, c$; $i = 1, 2, 3, 4$) denotes the i-th switching function of the middle-cell, and it is defined as

$$s_{xi} = \begin{cases} 1, & \text{when switch is ON} \\ 0, & \text{when switch is OFF.} \end{cases} \quad i = 1, 2, \ldots, 4 \tag{2}$$

According to (1), any required terminal voltage u_{xms} in the proposed middle-cell can be obtained by chopping u_{xucap} and u_{xlcap} with s_{x1} and s_{x2} at the appropriate switching frequency. Likewise, any required terminal voltage u_{xsn} can be obtained by chopping u_{xucap} and u_{xlcap} with s_{x3} and s_{x4}. Therefore, based on the terminal voltages and switching functions of the proposed middle-cell that are defined by (1) and (2), respectively, the terminal voltage u_{xmn} of the proposed middle-cell can be expressed as

$$\begin{aligned} u_{xmn} &= u_{xms} + u_{xsn} \\ &= (s_{x1} - s_{x3})\, u_{xucap} + (s_{x4} - s_{x2})\, u_{xlcap}. \end{aligned} \tag{3}$$

In terms of the modular nature and uniformity, the voltage references of the upper and lower capacitor voltages in the proposed middle cell are set to be equal. Meanwhile, since the power switches in a single arm of the proposed middle-cell are controlled with complementary signals, based on (1)–(3), there exists four switching states for the proposed middle-cell, as listed in Table I . When adopting the first two switching states for pulse driving, the proposed middle-cell changes only the feature of the ac equivalent model, while the dc equivalent model remains unchanged due to the zero voltage of u_{xmn}. However, when adopting the last two switching states for pulse driving, the nonzero feature of u_{xmn} introduces an uncontrollable peak voltage in phase control, resulting in a complex control system. Therefore, the first two switching states in Table I are preferred for the proposed middle-cell for achieving an excellent performance of the modified MMC.

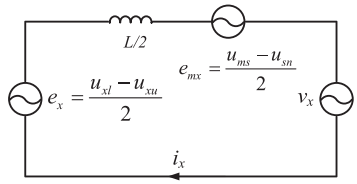

Fig. 3. AC equivalent model for single phase of the modified MMC.

According to Kirchhoff's voltage law, the mathematic model of the modified MMC system can be expressed as

$$\begin{cases} \frac{1}{2}V_{dc} - u_{xu} - u_{xms} - L\frac{di_{xu}}{dt} = v_x \\ -\frac{1}{2}V_{dc} + u_{xl} + u_{xsn} + L\frac{di_{xl}}{dt} = v_x \end{cases} \tag{4}$$

where u_{xu} and u_{xl} denote the upper and lower arm voltages of phase x ($x = a, b, c$), respectively, i_{xu} and i_{xl} denote the upper and lower arm currents of phase x ($x = a, b, c$), V_{dc} represents the dc bus voltage, L denotes the arm inductance, and v_x denotes the output voltage of phase x ($x = a, b, c$). Equation (4) shows that the terminal voltages u_{xms} and u_{xsn}, produced by the proposed middle-cell, change the circuit feature of the modified MMC. Through a deep study, and using a linear transformation of (4), the dc and ac equivalent math models of the modified MMC can be derived as follows:

$$\begin{cases} \frac{V_{dc} - u_{xu} - u_{xl}}{2} - \frac{u_{ms} + u_{sn}}{2} - L\frac{di_{xcir}}{dt} = 0 \\ \frac{u_{xl} - u_{xu}}{2} - \frac{u_{ms} - u_{sn}}{2} - \frac{L}{2}\frac{di_x}{dt} = v_x \end{cases} \tag{5}$$

where i_{xcir} denotes the circulating current of phase x ($x = a, b, c$), and i_x denotes the output current of phase x ($x = a, b, c$). The first and second equations in (5) represent the equivalent dc and ac mathematical models, respectively. When the first two switching states of the proposed middle-cell in Table I are applied, the sum of u_{xms} and u_{xsn} is always controlled to be zero, which means the proposed middle-cell will not change the performance of the dc equivalent mathematical model in (5). However, the distinct situation is introduced for the ac equivalent mathematical model. The schematic structure of the ac equivalent model is shown in Fig. 3, where, the inner electromotive force is denoted as e_x ($x = a, b, c$), and it consists of the upper and lower arm voltages, while e_{mx} ($x = a, b, c$) represents the contribution of the proposed middle-cell. According to (5), the compensated part e_{mx} contributed by u_{xms} and u_{xsn} serves as a controllable voltage source, which aims to produce the required voltage for improving the performance of the ac equivalent model in the modified MMC.

III. ANALYSIS AND CONTROL OF MODIFIED MMC SYSTEM

A. Analysis of the Modulation Process With THVI

The basic principle of the THVI is presented in Fig. 4, where it can be seen that the peak value of the arm reference voltage in the MMC system can be decreased by the THVI, which provides a possibility for enlarging the modulation index range. Theoretically, the maximum value of the modulation index of the half-bridge SM-based MMC can be increased up to 1.1547 by using the THVI [24]. However, due to the unconformity between the

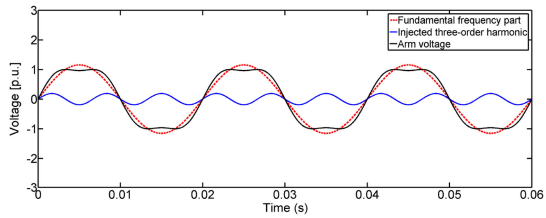

Fig. 4. Third-order harmonic voltage injection process.

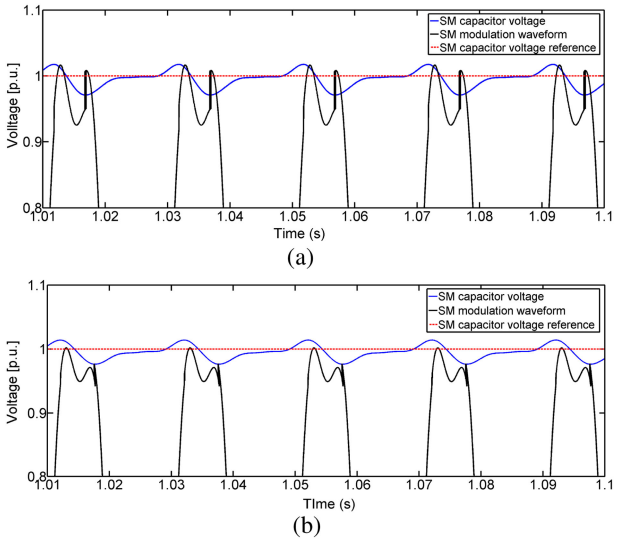

Fig. 5. Modulation process of SM capacitor voltage and arm voltage of the upper arm. (a) SM capacitor-voltage-reference based modulation process. (b) SM capacitor-voltage-ripple based modulation process.

arm output voltage and the arm voltage reference, the additional compensation parts produced by the circulating current control and balancing control are required, which changes the peak value of the arm voltages. Therefore, the theoretical maximum equivalent modulation index should be modified. The inserted third-order harmonic voltage is expressed as

$$v_h = V_h \sin 3\omega t \tag{6}$$

where V_h denotes the amplitude of the inserted third-order harmonic.

It is assumed that the SM capacitor voltages in the MMC system are well-balanced. Normally, the SM capacitor voltages in the upper and lower arms are supposed to be the same, respectively. The SM capacitor-voltage-reference based modulation process of a single SM under the THVI is presented in Fig. 5(a). By considering the compensation parts produced by the average control and balancing control, the SM modulation waveform is changed. As shown in Fig. 5(a), the peak value of the SM modulation waveform can exceed the SM capacitor voltage reference, leading to the overmodulation.

For avoiding the overmodulation phenomenon displayed in Fig. 5(a), the modulation waveform of the *i*-th SM can be normalized by the following:

$$m_{xyi} = \frac{u_{xsmy}}{u_{xcmy}} \tag{7}$$

where m_{xyi} denotes the *i*-th normalized SM modulation waveform of phase *x* ($x = a, b, c$; $y = u, l$), u_{xsmy} denotes the *i*-th SM modulation waveform, and u_{xcmy} denotes the *i*-th SM capacitor voltage of phase *x* ($x = a, b, c$; $y = u, l$). Based on (7), the SM modulation waveform can be controlled below the SM capacitor voltage ripple so as to avoid the overmodulation condition. The SM capacitor-voltage-ripple based modulation process, based on (7), is presented in Fig. 5(b), where it is shown that the maximum modulation index point can be tracked when the SM modulation waveform is extended to reach the peak value of the SM capacitor voltage ripple. It should be noted that, due to the unique charging process of the balancing control when the PSC-PWM [8] is adopted, an undesirable rush voltage appear in SM modulation waveform control as shown in Fig. 5, which changes the intersection point of the SM capacitor voltage ripple and the SM modulation waveform. A different form of (7) can be expressed as follows:

$$u_{xsmy} = m_{xyi} \cdot u_{xcmy} \tag{8}$$

Equation (8) indicates the influence of the SM capacitor voltage ripple on the SM output voltage has been considered. In other words, when producing a desirable SM output voltage, the normalized modulation waveform m_{xyi} changes in the opposite way compared to the SM capacitor voltage ripple. Thus, when the SM capacitor voltage is higher than the SM capacitor voltage reference, the normalized modulation waveform m_{xyi} decreases in order to support the desirable SM output voltage, and vice versa.

B. Analysis of the Arm Powers for Modified MMC

For simplification, only phase *a* of the modified MMC is analyzed in the following. Based on (6), the arm voltage reference of the modified MMC under the THVI can be expressed as

$$\begin{cases} u_{au-ref} = \frac{1}{2}V_{dc} - V_a \sin \omega t - V_h \sin 3\omega t \\ u_{al-ref} = \frac{1}{2}V_{dc} + V_a \sin \omega t + V_h \sin 3\omega t \end{cases} \tag{9}$$

where $u_{au\text{-}ref}$ and $u_{al\text{-}ref}$ denote the upper and lower arm voltage references, respectively, V_a denotes the amplitude of the output voltage of phase *a*, and ω represents the angular frequency of the output voltage. It is assumed that the circuit parameters of the upper and lower arms are highly consistent, so the output current can be evenly distributed in the upper and lower arms. Therefore, the arm currents of the modified MMC under the SHCI can be defined as follows:

$$\begin{cases} i_{au} = I_{acir} + \frac{1}{2}I_a \sin(\omega t - \varphi) + zI_{acir} \sin(2\omega t + \theta) \\ i_{al} = I_{acir} - \frac{1}{2}I_a \sin(\omega t - \varphi) + zI_{acir} \sin(2\omega t + \theta) \end{cases} \tag{10}$$

where i_{au} and i_{al} denote the upper and lower arm currents of phase *a*, respectively, I_{acir} denotes the dc part of the circulating current of phase *a*, I_a denotes the amplitude of the output current of phase *a*, φ denotes the phase angle difference between the output voltage and output current, z is defined as the second-order current harmonic index, θ denotes the phase angle of the second-order harmonic current, and $\theta \in [-\pi, \pi]$.

Combining (9) and (10), the instantaneous arm powers of the modified MMC can be obtained as

$$\begin{cases} p_{au} = p_{acom} + p_{adif} \\ p_{al} = p_{acom} - p_{adif} \end{cases} \tag{11}$$

where

$$\begin{cases} p_{acom} = \frac{m}{8} V_{dc} I_a \cos(2\omega t - \varphi) + \frac{zm}{8} V_{dc} I_a \sin(2\omega t + \theta) \\ - \frac{1}{4} V_h I_a \cos(2\omega t + \varphi) + \frac{1}{4} V_h I_a \cos(4\omega t - \varphi) \\ p_{adif} = \frac{2-m^2}{8} V_{dc} I_a \cos\varphi \sin\omega t - \frac{zm^2}{16} V_{dc} I_a \cos(\omega t + \theta) \\ - \frac{zm}{8} V_h I_a \cos(\omega t - \theta) - \frac{1}{4} V_{dc} I_a \sin\varphi \cos\omega t \\ + \frac{zm^2}{16} V_{dc} I_a \cos(3\omega t + \theta) - \frac{m}{4} V_h I_a \sin 3\omega t \\ + \frac{zm}{8} V_h I_a \cos(5\omega t + \theta) \end{cases} \tag{12}$$

where p_{au} and p_{al} denote the upper and lower arm powers of phase *a*, respectively, p_{acom} denotes the common part of the upper and lower arm powers of phase *a*, p_{adif} denotes the differential part of the upper and lower arm powers of phase *a*, and *m* is the modulation index that can be obtained by [15]. In order to achieve the maximum modulation index $m = 1.1547$, based on [23], the amplitude of the injected third-order harmonic voltage can be defined as

$$V_h = \frac{1}{6} V_a. \tag{13}$$

According to (12) and (13), the fundamental part of the arm powers in the modified MMC can be expressed as

$$p_{af} = \left(\frac{2-m^2}{8} V_{dc} I_a \cos\varphi + \frac{5zm^2}{96} V_{dc} I_a \sin\theta \right) \sin\omega t - \left(\frac{7zm^2}{96} V_{dc} I_a \cos\theta + \frac{1}{4} V_{dc} I_a \sin\varphi \right) \cos\omega t \tag{14}$$

where p_{af} denotes the fundamental part of the arm powers of phase *a*. Based on (14), the fundamental part of the arm powers can be eliminated when the following equations are satisfied:

$$\begin{cases} \frac{2-m^2}{8} \cos\varphi + \frac{5zm^2}{96} \sin\theta = 0 \\ \frac{7zm^2}{96} \cos\theta + \frac{1}{4} \sin\varphi = 0. \end{cases} \tag{15}$$

When the modified MMC operates under the unit power factor ($\varphi = 0$), the second equation in (15) is valid only when $\cos\theta = 0$, which yields to

$$\theta = \pm \frac{\pi}{2}. \tag{16}$$

Moreover, the modulation index and the second-order current harmonic index are limited by

$$\begin{cases} 0 \le m \le 1.1547 \\ z \ge 0. \end{cases} \tag{17}$$

Therefore, according to (15)-(17), the first equation in (15) is valid only when $\sin\theta < 0$ under unit the power factor ($\varphi = 0$), which yields to

$$\theta = -\frac{\pi}{2}. \tag{18}$$

By substituting (18) and $\varphi = 0$ into (15), p_{af} under the unit power factor can be eliminated when the following condition is satisfied

$$4 = \left(2 + \frac{5}{6} z\right) m^2. \tag{19}$$

When the modified MMC operates at other power factors, (15) can be expressed as

$$\begin{cases} z \sin\theta = -\frac{12}{5} \frac{2-m^2}{m^2} \cos\varphi \\ z \cos\theta = -\frac{24}{7m^2} \sin\varphi. \end{cases} \tag{20}$$

Based on (20), the relationship between θ, φ, and *m* when $\varphi \neq 0$ can be obtained as follows

$$\tan\theta = \frac{7}{10} \left(2 - m^2\right) \cot\varphi. \tag{21}$$

Based on (21), once the modulation index is specified when $\varphi \neq 0$, the phase angle of the injected second-order harmonic current can be calculated by the phase angle of the output voltage and the output current. Then, the second-order harmonic current index can be calculated by (20).

Table II lists the relationships between θ, φ, and z at $m = 1.1547$ when the fundamental part of the arm powers is eliminated. It shows that the second-order harmonic current index z and the absolute value of θ increase with φ. Therefore, the minimum value of z can be obtained when the modified MMC operates at the unit power factor. Particularly, since the MMC system is usually controlled at nearly unit power factor, the arm powers of the modified MMC operating under the unit power factor have been mainly analyzed. When transferring only the active power, the arm powers of the modified MMC can be expressed as

TABLE II
RELATIONSHIPS BETWEEN φ, θ, AND Z WHEN M = 1.1547

φ	0	0.028π	0.056π	0.083π	0.111π
θ	-0.5π	-0.561π	-0.617π	-0.667π	-0.711π
z	1.20	1.22	1.26	1.34	1.43

$$\begin{cases} p_{acom} = \frac{(1-z)m}{8} V_{dc} I_a \cos 2\omega t - \frac{1}{4} V_h I_a \cos 2\omega t \\ \quad + \frac{1}{4} V_h I_a \cos 4\omega t \\ p_{adif} = \frac{4-(2+z)m^2}{16} V_{dc} I_a \sin\omega t + \frac{zm}{8} V_h I_a \sin\omega t \\ + \frac{zm^2}{16} V_{dc} I_a \sin 3\omega t - \frac{m}{4} V_h I_a \sin 3\omega t + \frac{zm}{8} V_h I_a \sin 5\omega t \end{cases} \tag{22}$$

Based on (19), the variation of the second-order current harmonic index with the modulation index under the unit power factor in the modified MMC is depicted in Fig. 6. As shown in Fig. 6, the second-order current harmonic index z decreases when the modulation index increases. Especially, the second-order current harmonic index is two times larger at $m = 1$ than at $m = 1.1547$. Therefore, the minimum value of the second-order current harmonic index can be obtained when the modulation index is equal to its maximum value $m_{\max}$. Therefore, based on (19), it yields to

$$\begin{cases} m_{\max} = 1.1547 \\ z_{\min} = 1.2. \end{cases} \tag{23}$$

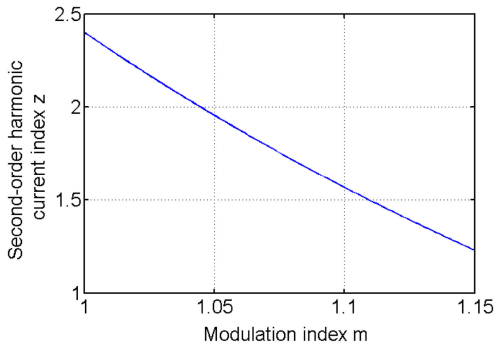

Fig. 6. Second-order harmonic current index of the modified MMC varied with modulation index under unit power factor.

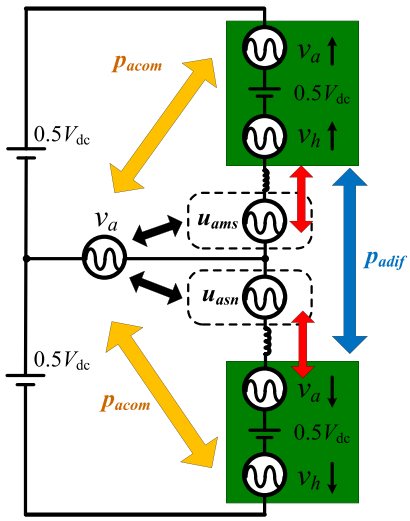

Fig. 7. Power distribution of the modified MMC under the THVI.

Combining (13), (22), and (23), the following expressions can be derived

$$\begin{cases} p_{acom} = \frac{m_{\max}}{8} V_{dc} I_a \cos 2\omega t - \frac{z_{\min} m_{\max}}{8} V_{dc} I_a \cos 2\omega t \\ \quad - \frac{m_{\max}}{48} V_{dc} I_a \cos 2\omega t + \frac{m_{\max}}{48} V_{dc} I_a \cos 4\omega t \\ p_{adif} = \frac{z_{\min} m_{\max}^2}{16} V_{dc} I_a \sin 3\omega t - \frac{m_{\max}^2}{48} V_{dc} I_a \sin 3\omega t \\ \quad + \frac{z_{\min} m_{\max}^2}{96} V_{dc} I_a \sin 5\omega t. \end{cases} \tag{24}$$

Based on (24), the fundamental parts of the arm powers of the modified MMC have been eliminated, and the dominant powers in the SMs are the second-order harmonics. Meanwhile, (14) also shows that the second term in p_{acom}, the first term in p_{adif}, and the third term in p_{adif} express the contribution by the SHCI.

C. Power Distribution Analysis of the Modified MMC

The power distribution of the modified MMC under the THVI is presented in Fig. 7. It is assumed that the high frequency harmonics caused by switching pulses are neglected, so the upper arm voltage can be expressed as the formation of $0.5V_{\rm dc}$, $-v_x$, and $-v_{\rm h}$, while the lower arm voltage can be expressed as the formation of $0.5V_{\rm dc}$, v_x, and $v_{\rm h}$. u_{xms} and u_{xsn} $(x = a, b, c)$ denote the compensated parts generated by the proposed middle-cells for the upper and lower arms of the modified MMC, respectively. As shown in Fig. 7, the arm voltages and the corresponding compensated part produced by the proposed middle-cell can be integrated into an equivalent arm of the modified MMC, which shows the same external characteristic as that of the traditional MMC topology.

As depicted in Fig. 7, the HBSMs and the proposed middle-cells act as the medium platform for power exchanging between the dc and ac sides. In the modified MMC system, the dc source delivers the active powers to the HBSMs, which are sent to the loads instantly. At the same time, the first and second terms in the right hand of $p_{\rm acom}$ in (24) are delivered from the HBSMs to the loads, and the third and fourth terms in the right hand of $p_{\rm acom}$ in (24) flow back and forth between the HBSMs and proposed middle-cells. The first term in the right hand of $p_{\rm adif}$ in (24) is controlled to flow back and forth between the upper arm HBSMs and lower arm HBSMs, while the second and third terms in the right hand of $p_{\rm adif}$ in (24) are controlled to exchange powers between the HBSMs and proposed middle-cells.

D. Analysis of the SM Capacitor Voltage Ripples

In [15], it has been verified that the arm powers and SM capacitor voltage ripples contain the same frequency components of the MMC system, and the amplitude of the *i*-th harmonic in the SM capacitor voltage ripple can be calculated by the *i*-th harmonic of the arm powers [15]. Therefore, according to (24), the SM capacitor voltages of the modified MMC can be expressed as

$$\begin{cases} u_{acmu} = u_{ref} + u_{acom} + u_{adif} \\ u_{acml} = u_{ref} + u_{acom} - u_{adif} \end{cases} \tag{25}$$

where

$$\begin{cases} u_{acom} = \frac{(1-z_{\min}) m_{\max}}{16 C\omega U_{ref} n} V_{dc} I_a \sin 2\omega t - \frac{m_{\max}}{96 C\omega U_{ref} n} V_{dc} I_a \sin 2\omega t \\ \quad + \frac{m_{\max}}{192 C\omega U_{ref} n} V_{dc} I_a \sin 4\omega t \\ u_{adif} = \frac{-z_{\min} m_{\max}^2}{48 C\omega U_{ref} n} V_{dc} I_a \cos 3\omega t + \frac{m_{\max}^2}{144 C\omega U_{ref} n} V_{dc} I_a \cos 3\omega t \\ \quad - \frac{z_{\min} m_{\max}^2}{480 C\omega U_{ref} n} V_{dc} I_a \cos 5\omega t \end{cases} \tag{26}$$

where u_{acmu} and u_{acml} denote the upper and lower SM capacitor voltages of phase a, respectively, u_{ref} denotes the SM capacitor voltage reference, u_{acom} represents the common part of u_{acmu} and u_{acml}, and u_{adif} represents the differential part of u_{acmu} and u_{acml}. According to (26), the SM capacitor voltage ripple of the modified MMC mainly contains four different frequency components. The second-order harmonics in u_{acom} and the third-order harmonics in u_{adif} are dominant in the SM capacitor voltage ripple, while the fourth- and fifth-order harmonics in (26) have slight significance in SM capacitor voltage ripple.

Based on (26), the SM capacitor voltage ripple function of the modified MMC can be derived as

$$\varepsilon_1 \approx \frac{-1.27\sin 2\omega t + 0.289 \sin 4\omega t \mp 1.156 \cos 3\omega t \mp 0.16 \cos 5\omega t}{48 C\omega U_{ref} n} \times V_{dc} I_a \tag{27}$$

where ε_1 denotes the SM capacitor voltage ripple function of the modified MMC under the proposed scheme, and sign $\mp$ contributes to the upper arm and lower arm capacitor voltage ripple. Accordingly, the peak-to-peak value of the SM capacitor voltage ripple in (27) can be expressed as

$$\lambda_1 = \max(\varepsilon_1) - \min(\varepsilon_1) \approx \frac{8.61 V_a I_a}{48 C\omega U_{ref} n} \tag{28}$$

where λ_1 denotes the peak-to-peak value of the SM capacitor voltage ripple function ε_1.

Meanwhile, aiming to verify the effectiveness of the proposed method in the modified MMC, it is necessary to calculate the SM capacitor voltage under the traditional MMC topology. For the sake of fair comparison, the traditional and modified MMCs should operate under equal modulation index and system power. Therefore, the SM capacitor voltage of the traditional MMC under the THVI is calculated by

$$\begin{cases} u_{acom} = \frac{5m}{96C\omega U_{ref} n} V_{dc} I_a \sin 2\omega t + \frac{m}{192C\omega U_{ref} n} V_{dc} I_a \sin 4\omega t \\ u_{adif} = -\frac{2-m^2}{8C\omega U_{ref} n} V_{dc} I_a \cos \omega t + \frac{m^2}{144C\omega U_{ref} n} \\ V_{dc} I_a \cos 3\omega t \end{cases} \tag{29}$$

Similarly, based on (29), the peak-to-peak value of the SM capacitor voltage ripple at $m = 1.1547$ can be expressed as

$$\varepsilon_2 \approx \frac{\mp 4\cos \omega t + 2.887 \sin 2\omega t \pm 0.444 \cos 3\omega t + 0.289 \sin 4\omega t}{48 C\omega U_{ref} n} V_{dc} I_a \tag{30}$$

where ε_2 denotes the SM capacitor voltage ripple function of the traditional MMC under the THVI. Based on (29), the peak-to-peak value of ε_2 can be given as

$$\lambda_2 = \max(\varepsilon_2) - \min(\varepsilon_2) \approx \frac{21.75 V_a I_a}{48 C\omega U_{ref} n} \tag{31}$$

where λ_2 denotes the peak-to-peak value of the SM capacitor voltage ripple function ε_2.

According to (30), the fundamental part denotes the dominant part in the SM capacitor voltage ripple of the traditional MMC, which is mainly contributed by differential-mode powers in arm powers [8]. However, by power redistribution in the modified MMC using the proposed method, the SM capacitor voltage ripples in (27) are mainly influenced by the common-mode power p_{acom} and differential power p_{adif}. By comparing (28) and (31), it can be concluded that in the modified MMC, a significant reduction of the SM capacitor voltage ripple can be achieved.

E. Analysis of the Proposed Middle-Cell

As explained in Section II, the undesirable common-mode voltages caused by the THVI appear on the AC side. Aiming to solve this problem, the voltage reference of the proposed middle-cell in the modified MMC can be defined as

$$\begin{cases} u_{xms} = V_h \sin 3\omega t \\ u_{xsn} = -V_h \sin 3\omega t. \end{cases} \tag{32}$$

Considering (32) and the first two switching states in Table I, the driving signals of the power switches in the proposed middle-cells can be defined. Therefore, the currents of the left arm in the proposed middle-cells split the upper arm currents with the specified proportion, which can be expressed as

$$\begin{cases} i_{xlup} = -\frac{1}{2}\left(1 + \frac{V_h}{2U_{ref}} \sin 3\omega t\right) \cdot i_{xu} \\ i_{xllow} = \frac{1}{2}\left(1 - \frac{V_h}{2U_{ref}} \sin 3\omega t\right) \cdot i_{xu} \end{cases} \tag{33}$$

where i_{xlup} and i_{xllow} denote the upper and lower arm currents of the left arm in the proposed middle-cell of phase x ($x = a, b, c$), respectively, and i_{xu} denotes the upper arm current of phase x ($x = a, b, c$).

Similarly, the currents in the right arm of the proposed middle-cell can be expressed as

$$\begin{cases} i_{xrup} = \frac{1}{2}\left(1 + \frac{V_h}{2U_{ref}} \sin 3\omega t\right) \cdot i_{xl} \\ i_{xrlow} = -\frac{1}{2}\left(1 - \frac{V_h}{2U_{ref}} \sin 3\omega t\right) \cdot i_{xl} \end{cases} \tag{34}$$

where i_{xrup} and i_{xrlow} denote, respectively, the upper and lower arm currents of the right arm in the proposed middle cell of phase x ($x = a, b, c$), respectively, and i_{xl} denotes the lower arm current of phase x ($x = a, b, c$). For simplification, the analysis of the proposed middle-cell for phase a is provided. According to (10), (33), and (34), the capacitor currents in the proposed middle cell are given as

$$\begin{cases} i_{aucap} = -i_{alup} - i_{arup} = \frac{1}{2} I_a \sin(\omega t - \varphi) \\ \quad + \frac{V_h I_a}{8U_{ref}} \cos(2\omega t + \varphi) - \frac{V_h}{8U_{ref}} \cos(4\omega t - \varphi) \\ i_{alcap} = -i_{allow} - i_{arlow} = -\frac{1}{2} I_a \sin(\omega t - \varphi) \\ \quad + \frac{V_h I_a}{8U_{ref}} \cos(2\omega t + \varphi) - \frac{V_h I_a}{8U_{ref}} \cos(4\omega t - \varphi) \end{cases} \tag{35}$$

where i_{aucap} and i_{alcap} denote, respectively, the upper and lower arm currents of the capacitor arm in proposed middle-cell of phase a. Based on (35), the output current is evenly split between the upper and lower capacitor currents in the proposed middle-cell. Thus, the fundamental component with same amplitude, but the opposite sign, will appear in the upper and lower capacitor voltage ripples of the proposed middle-cell. Meanwhile, due to the common parts of i_{aucap} and i_{alcap} in (35), the same voltage ripple on capacitor voltage appears in the proposed middle-cell. Therefore, according to (35) and the above discussion, the capacitor voltages in the proposed middle-cell can be expressed as

$$\begin{cases} u_{aucap} = U_{ref} + u_{amcom} + u_{amdif} \\ u_{alcap} = U_{ref} + u_{amcom} - u_{amdif} \end{cases} \tag{36}$$

where

$$\begin{cases} u_{amcom} = \frac{V_h I_a}{16C\omega U_{ref}} \sin(2\omega t + \varphi) - \frac{V_h I_a}{32C\omega U_{ref}} \sin(4\omega t - \varphi) \\ u_{amdif} = -\frac{I_a}{2C\omega} \cos(\omega t - \varphi) \end{cases} \tag{37}$$

where u_{aucap} and u_{alcap} denote, respectively, the upper and lower capacitor voltages of the proposed middle-cell of phase a, u_{amcom} represents the common part of u_{aucap} and u_{alcap}, u_{amdif} represents the differential part of u_{aucap} and u_{alcap}, and U_{ref} denotes the capacitor voltage reference of the proposed

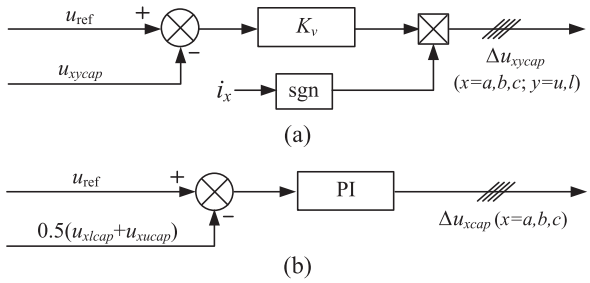

Fig. 8. Control of the proposed middle cell. (a) Balancing control of the capacitor voltages. (b) Average control of the capacitor voltages.

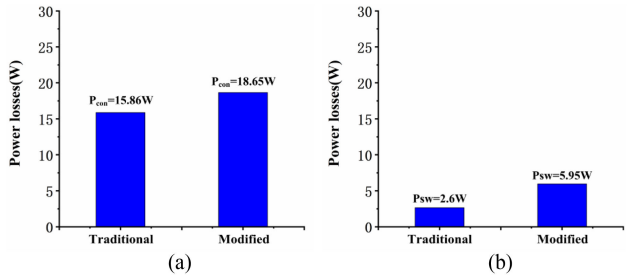

Fig. 9. Power losses of the traditional and modified MMCs. (a) Conduction losses. (b) Switching losses.

middle-cell. In (37), the fundamental parts of the upper and lower arm capacitor voltage ripples have the same amplitude but the opposite sign. However, the second and fourth-order harmonics in (37) are equal for u_{aucap} and u_{alcap}, and they are much smaller than the fundamental part in (37).

F. Control of the Proposed Middle-cell

The control structure of the proposed middle-cell of the modified MMC is presented in Fig. 8, where it can be seen that it includes the average control and balancing control. In the balancing control of the proposed middle-cell that is shown in Fig. 8(a), the compensated active powers, absorbed from the output current, are proposed for the modulation waveforms of the proposed middle-cells once the capacitor voltages of the proposed middle-cell deviate from the voltage reference. However, as shown in Fig. 2(b), the capacitor currents are contributed by both the left arm and the right arm of the proposed middle-cell, which means using only the balancing control is not sufficient for balancing the capacitor voltages. Therefore, the average control of the proposed middle-cell is introduced, and it is shown in Fig. 8(b).

According to the above discussion, the voltage reference of the proposed middle-cell can be expressed as

$$u_{xmid} = V_h \sin 3\omega t + \Delta u_{xucap} + \Delta u_{xlcap} + \Delta u_{xcap} \quad (38)$$

where u_{xmid} denotes the voltage reference of the proposed middle-cell of phase x ($x = a, b, c$), Δu_{xycap} ($y = u, l$) denotes the compensation part produced by the balancing control, and Δu_{xcap} ($x = a, b, c$) denotes the compensation part produced by the average control. As discussed in Section II, the terminal voltage u_{xms} in the proposed middle-cell is obtained by chopping s_{x1} and s_{x2}. Therefore, by considering the influence of the control system, the driving signals of the left arm in the proposed middle-cell for achieving desirable u_{xms} can be obtained by (38). Meanwhile, since the first two switching states in Table I are selected, the switching signals of s_{x3} and s_{x4} in the proposed middle-cell are driven with the same signals of s_{x1} and s_{x2} for producing desirable u_{xsn}.

G. Power Losses Analysis

One of the differences between the traditional and modified MMCs is the arm current waveform. Therefore, at the same load, the arm currents of the modified MMC contain the additional second-order harmonic currents in comparison to the arm currents of the traditional MMC. Meanwhile, due to the additional power losses caused by the proposed middle-cells, both conduction and switching losses in the modified MMC are larger than those in the traditional MMC. The calculation results of the conduction and switching losses of the traditional and modified MMCs are presented in Fig. 9. The parameters in Fig. 9 are the same as those in the simulations, all the semiconductor devices are at $T_{vj} = 25°C$ and $V_{GE} = 15V$ (Type of the IGBT module in experiment is FF150R12ME3G).

TABLE III
CIRCUIT PARAMETERS FOR SIMULATION

Symbol	Quantity	Value
V_{dc}	Dc-link voltage	200V
N	Number of SMs per arm	4
C	SM capacitor	1mF
C_{mid}	Middle-cell capacitor	2mF
L	Arm inductor	10mH
f_c	SM switching frequency	1kHz
f_{fc}	Middle-cell switching frequency	10kHz
f	Fundamental frequency	50Hz
u_{cm}	SM capacitor voltage reference	50V
U_{mid}	Middle-cell capacitor voltage reference	50V
R_{load}	Load resistance	50Ω

IV. SIMULATION RESULTS

The detailed mathematical model and SM features of the modified MMC have been analyzed in Section II. In order to verify the effectiveness of the above discussion, the simulation of the modified MMC is performed under MATLAB/Simulink. Aiming to obtain the superior output voltage and maintain an evenly harmonic distribution among the SM output voltages, the phase-shifted carrier PWM (PSC-PWM) is adopted [8]. Detailed simulation parameters are listed in Table III.

For the sake of fair comparison, the SM capacitor voltages of the traditional MMC under the THVI are simulated at $m = 1.1547$. The SM capacitor voltages of the traditional and modified MMCs are presented in Fig. 10. As shown in Fig. 10(a), the peak-to-peak value of the SM capacitor voltage ripple of the traditional MMC is 2.1V, while that of the modified MMC is 0.9V as shown in Fig. 10(b); thus, a significant reduction in the SM capacitor voltage ripple is achieved by the modified MMC. The spectrum distributions of the SM capacitor voltages are

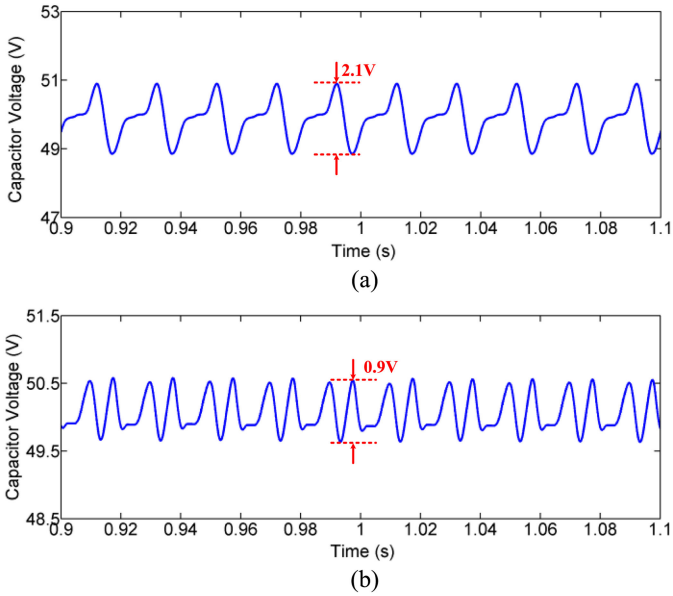

Fig. 10. SM capacitor voltages with the THVI. (a) Traditional MMC. (b) Modified MMC.

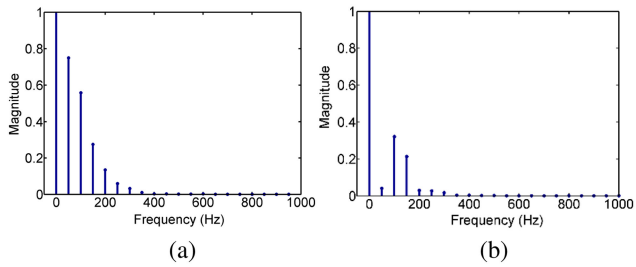

Fig. 11. Spectrum distribution of SM capacitor voltage. (a) Spectrum distribution of the SM capacitor voltage in traditional MMC with the THVI. (b) Spectrum distribution of the SM capacitor voltage in modified MMC with the THVI.

TABLE IV
PEAK TO PEAK VALUE OF SM CAPACITOR VOLTAGE RIPPLE

Type	Theoretical results	Simulation results
Modified MMC	0.76V	0.9V
Traditional MMC	1.93V	2.1V

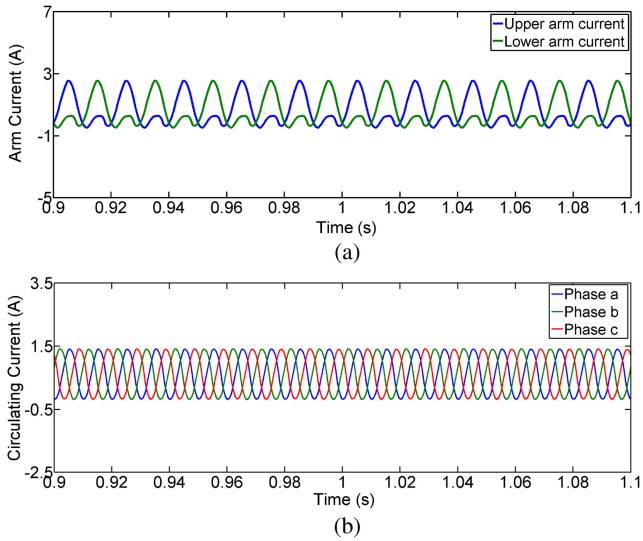

Fig. 12. Currents of the modified MMC. (a) Arm currents of the modified MMC. (b) Circulating currents of the modified MMC.

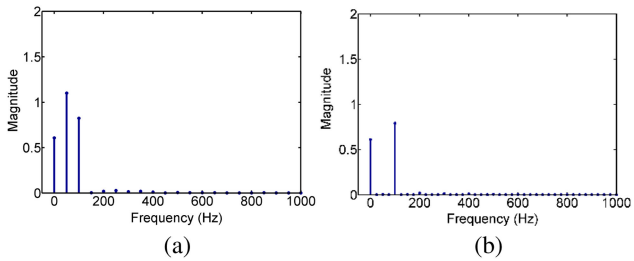

Fig. 13. Spectrum distribution of the currents in modified MMC. (a) Spectrum distribution of the arm current. (b) Spectrum distribution of the circulating current.

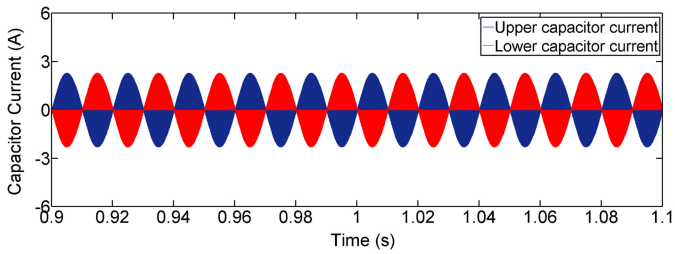

Fig. 14. Capacitor currents of the middle-cell in the modified MMC.

displayed in Fig. 11. Fig. 11(a) shows the spectrum distribution of Fig. 10(a), and Fig. 11(b) shows the spectrum distribution of Fig. 10(b). As shown in Fig. 11(a), the dominant ripple in the SM capacitor voltage is the fundamental part. However, in the modified MMC, the fundamental part in the SM capacitor voltage ripple is basically eliminated as shown in Fig. 11(b). Moreover, the theoretical calculations obtained by (28) and (31) and simulated results of the SM capacitor voltage ripple of the modified and traditional MMCs are listed in Table IV , where a good agreement between the theoretical and simulation results can be observed.

The arm currents and the corresponding spectrum distribution of the modified MMC are depicted in Figs. 12(a) and 13(a), respectively, where it can be seen that the arm currents mainly consist of the dc part, fundamental part and the second-order harmonic part. The circulating current and the corresponding spectrum distribution of the modified MMC are shown in Figs. 12(b) and 13(b), respectively, where it can be seen that the circulating current mainly contains the dc part and the second-order harmonic. The simulation results in Figs. 12 and 13 are basically in accordance with the calculation results obtained by (10).

According to the power distribution in Fig. 7, the proposed middle-cells in the modified MMC serve as a medium platform for power transfer between the upper arm, lower arm and ac side. The capacitor currents of the proposed middle-cell are shown in Fig. 14. The spectrum distribution of the capacitor current in

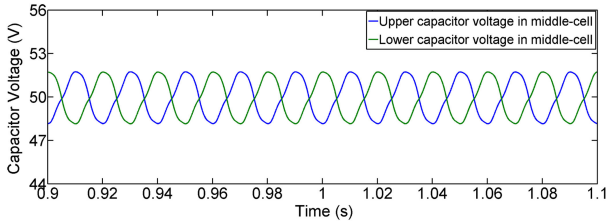

Fig. 15. Capacitor voltages of the middle-cell in the modified MMC.

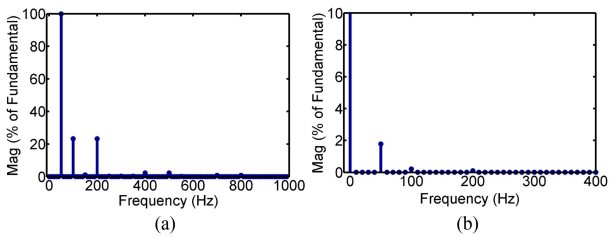

Fig. 16. Spectrum distribution of the middle-cell. (a) Spectrum distribution of the capacitor current in the middle-cell (b) Spectrum distribution of the capacitor voltage in the middle-cell.

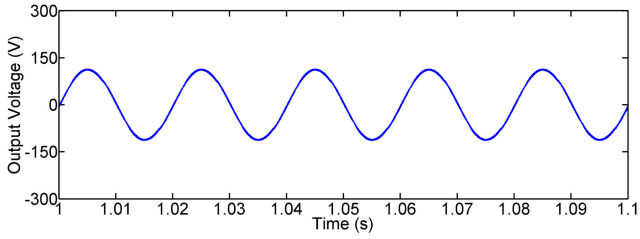

Fig. 17. Output voltage of the modified MMC with the THVI.

the proposed middle-cell is shown in Fig. 16(a), where it can be seen that the capacitor currents in the proposed middle-cell consist of the fundamental part, second-order and fourth-order harmonics, which highly is coincidental with the discussion in (35). The capacitor voltages in the proposed middle-cell of the modified MMC are shown in Fig. 15, and the corresponding spectrum distribution is shown in Fig. 16(b). It shows that the fundamental parts of the upper and lower capacitor voltages of the proposed middle-cell have equal amplitude but opposite sign, which is consistent with the calculated results in (37).

The results show that the THVI can increase the utilization of the dc bus voltage in the MMC system, but it introduces undesirable common-mode voltages on the ac side. However, in the modified MMC, by proper control of the proposed middle-cells, the influence of the THVI on the ac side can be significantly improved. Generally, the common-mode voltages are not directly imposed in the output voltages. The output voltage of the modified MMC with the THVI is presented in Fig. 17. The common-mode voltage caused by the THVI in the MMC system is displayed in Fig. 18. The common-mode voltage of the traditional MMC topology is shown in Fig. 18(a), where an undesirable dominant third-order harmonic voltage can be observed. However, in the modified MMC, the compensation part produced by the proposed middle-cell is used to eliminate the undesirable third-order harmonic voltage, as shown

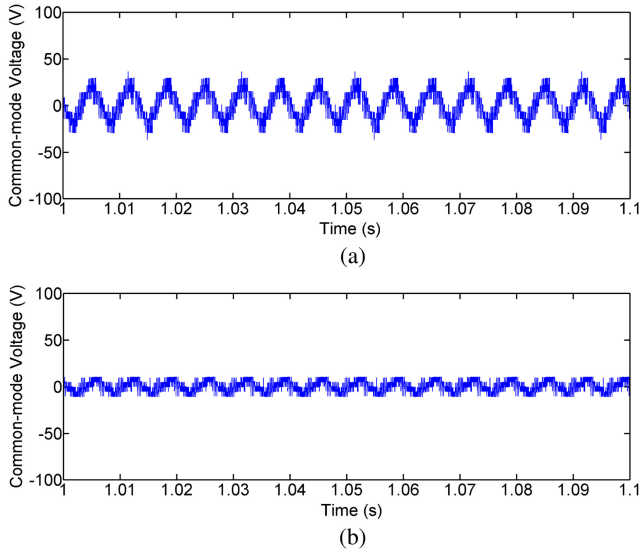

Fig. 18. Common-mode voltages in MMC. (a) Common-mode voltage with the THVI in traditional MMC. (b) Common-mode voltage with the THVI in modified MMC.

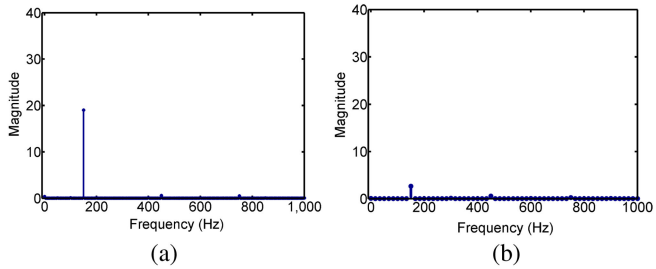

Fig. 19. Spectrum distribution of the common-mode voltage. (a) Spectrum distribution of the common-mode voltage in the traditional MMC with the THVI. (b) Spectrum distribution of the common-mode voltage in the modified MMC with the THVI.

in Fig. 18(b); the corresponding spectrum distributions of the common-mode voltages are shown in Fig. (19), where it can be seen that the common-mode voltage in the modified MMC can be mostly suppressed compared with that in the traditional MMC.

V. Experimental Results

The downscaled power prototype of the modified MMC is built to verify the effectiveness of the discussion. Due to the limitation of the experimental facilities, the monophase power stage with four SMs per arm is established. Fig. 20 is the basic construction of the modified MMC system. It consists of the power stage and the control system. The modified MMC is operated at inverter mode, which is fed by the dc source composed by a three-phase uncontrollable rectifier. Fig. 21 shows the control system, which consists of a TI-tms320f28335 DSP chip and an Altera EP4CE115F23C8N FPGA chip. The DSP chip in the control system serves as the host one to achieve the control algorithm, while the FPGA chip sends the required signals to the DSP chip and produces the PWM signals for the power switches. The whole photograph of the experimental circuit is shown

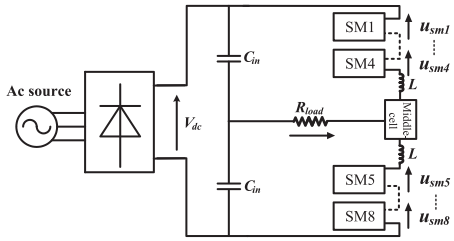

Fig. 20. Experimental structure of the modified MMC.

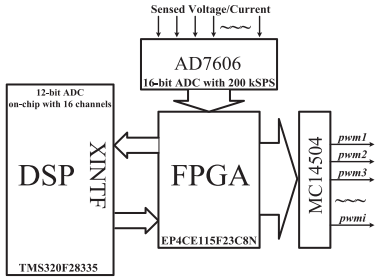

Fig. 21. Diagram of the control system.

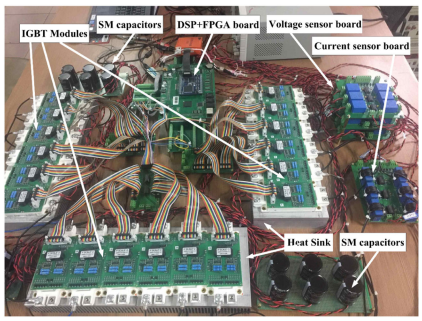

Fig. 22. Experimental photograph of the modified MMC.

in Fig. 22. The detailed experimental parameters are listed in Table V.

The experimental results of the SM capacitor voltages of the traditional and modified MMCs are presented in Fig. 23. As depicted in Fig. 23(a), the peak-to-peak value of the SM capacitor voltage ripple of the traditional MMC is 4V, while that of the modified MMC is 1.95V, as shown in Fig. 23(b). Obviously, the modified MMC shows better performance in SM capacitor voltage ripple reduction. As discussed in Section III, this is mainly due to the inserted second-order harmonic currents given by (10), which provided the power degree of freedom under the THVI for eliminating the dominant harmonics in arm powers. The corresponding arm currents of the modified MMC are shown in Fig. 24, which shows the nonsinusoidal feature.

The experimental results of the capacitor voltages of the proposed middle-cell in the modified MMC are shown in Fig. 25, where it can be seen that the upper and lower arm capacitor voltages in the proposed middle-cell contain the opposite voltage ripples, which verifies the theoretical analysis and relationships given in (36) and (37). Finally, under the proposed control, the output voltage and current of the modified MMC are shown in Fig. 26.

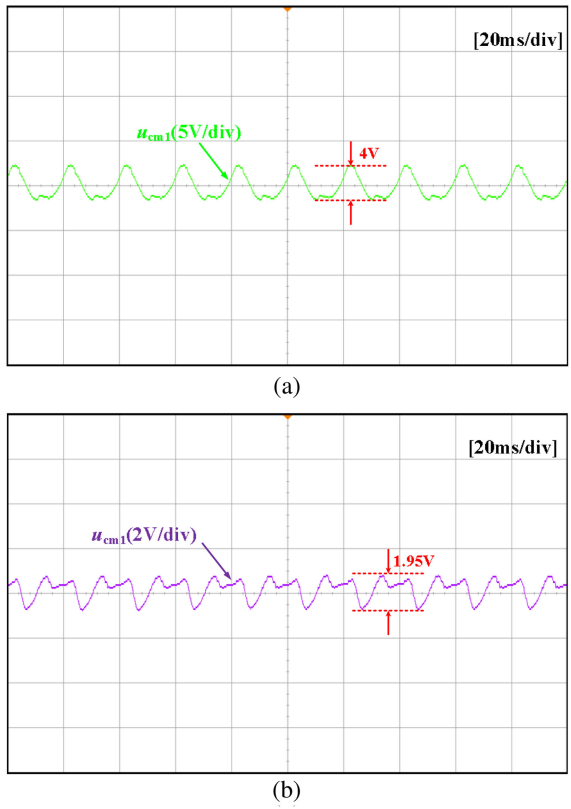

Fig. 23. Experimental results of the SM capacitor voltage. (a) SM capacitor voltage of traditional MMC. (b) SM capacitor voltage of modified MMC.

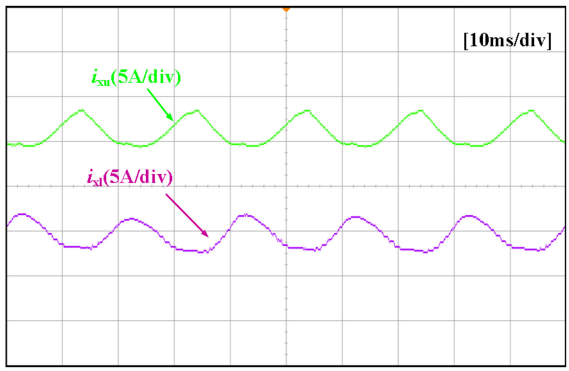

Fig. 24. Experimental results of the arm currents of the modified MMC.

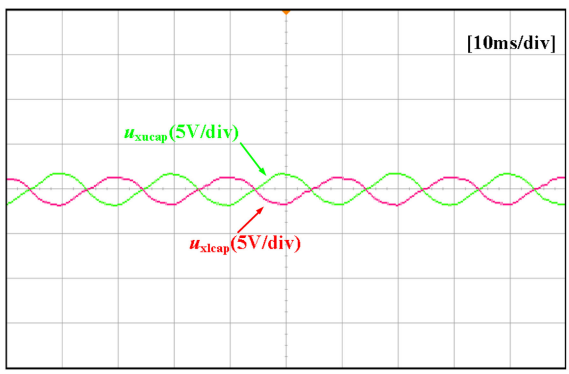

Fig. 25. Experimental results of the middle cell capacitor voltages in modified MMC.

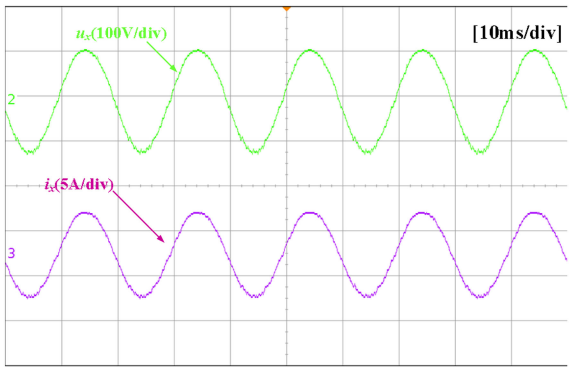

Fig. 26. Experimental results of the output voltage and current in modified MMC.

VI. Conclusion

This article presents a modified MMC topology based on proposed middle-cells, which aims to achieve a large reduction in the SM capacitor voltage ripple under the THVI and SHCI without common-mode voltage injected on the ac side. First, the arm power analysis of the modified MMC under the THVI and SHCI using different power factors is provided. It is found that the modified MMC operating at a reduced power factor requires a larger amplitude of the second-order harmonic current when eliminating the fundamental part of the SM capacitor voltage ripple. In addition, the increased modulation index results in the decreased amplitude of the second-order harmonic of the circulating current. The minimum value of the amplitude of the second-order harmonic current can be obtained when the modified MMC operates at the unit power factor, which can limit the power losses to the acceptable range. Meanwhile, the analysis and control of the proposed middle-cell in the modified MMC is also presented. The analysis result shows that the common-mode voltage caused by the THVI can be basically suppressed by the proposed middle-cells of the modified MMC. The effectiveness of the theoretical analysis of the modified MMC is verified by the simulation and experimental results.

References

[1] A. Lesnicar and R. Marquardt, "An innovative modular multilevel converter topology suitable for a wide power range," in *Proc. IEEE Power Tech Conf.*, Jun. 2003, pp. 1–6.

[2] M. Glinka and R. Marquardt, "A new AC/AC multilevel converter family," *IEEE Trans. Ind. Electron.*, vol. 52, no. 3, pp. 662–669, Jun. 2005.

[3] M. Glinka, "Prototype of multiphase modular-multilevel converter with 2 MW power rating and 17-level-output-voltage," in *Proc. IEEE Power Electron. Spec. Conf. (PESC)*, 2004, pp. 2572–2576.

[4] H. Akagi, "Classification, terminology, and application of the modular multilevel cascade converter (MMCC)," *IEEE Trans. Power Electron.*, vol. 26, no. 11, pp. 3119–3130, Nov. 2011.

[5] M. Zhang, L. Huang, W. Yao, and Z. Liu, "Circulating harmonic current elimination of a CPS-PWM-Based modular multilevel converter with a Plug-in repetitive controller," *IEEE Trans. Power Electron.*, vol. 29, no. 4, pp. 2083–2097, Apr. 2014.

[6] S. Li, X. Wang, Z. Yao, T. Li, and Z. Peng, "Circulating current suppressing strategy for MMC-HVDC based on nonideal proportional resonant controllers under unbalanced grid conditions," *IEEE Trans. Power Electron.*, vol. 30, no. 1, pp. 387–397, Jan. 2015.

[7] Y. Sun, C. A. Teixeira, D. G. Holmes, B. P. McGrath, and J. Zhao, "Low-order circulating current suppressing of PWM-Based modular multilevel converters using DC-Link voltage compensation," *IEEE Trans. Power Electron.*, vol. 33, no. 1, pp. 210–225, Jan. 2018.

[8] M. Hagiwara and H. Akagi, "Control and experiment of pulse width-modulated modular multilevel converters," *IEEE Trans. Power Electron.*, vol. 24, no. 7, pp. 1737–1746, Jul. 2009.

[9] F. Deng and Z. Chen, "Voltage-Balancing method for modular multilevel converters under phase-shifted carrier-based pulse width modulation," *IEEE Trans. Power Electron.*, vol. 62, no. 7, pp. 4158–4169, Jul. 2015.

[10] D. Siemaszko, "Fast sorting method for balancing capacitor voltages in modular multilevel converters," *IEEE Trans. Power Electron.*, vol. 30, no. 1, pp. 463–470, Jan. 2015.

[11] M. Huang, J. Zou, and X. Ma, "An improved phase-shifted carrier modulation for modular multilevel converter to suppress the influence of fluctuation of capacitor voltage," *IEEE Trans. Power Electron.*, vol. 30, no. 1, pp. 7404–7416, Oct. 2016.

[12] S. Fan, K. Zhang, J. Xiong, and Y. Xue, "An improved control system for modular multilevel converters with new modulation strategy and voltage balancing control," *IEEE Trans. Power Electron.*, vol. 30, no. 1, pp. 358–371, Jan. 2015.

[13] Z. Li, P. Wang, H. Zhu, Z. Chu, and Y. Li, "An improved pulse width modulation method for chopper-cell-based modular multilevel converters," *IEEE Trans. Power Electron.*, vol. 27, no. 8, pp. 3472–3481, Aug. 2012.

[14] M. Hagiwara, K. Nishimura, and H. Akagi, "A medium-voltage motor drive with a modular multilevel PWM inverter," *IEEE Trans. Power Electron.*, vol. 25, no. 7, pp. 1786–1799, Jul. 2010.

[15] M. Huang, J. Zou, and X. Ma, "Hybrid modular multilevel converter with redistributed power to reduce submodule capacitor voltage fluctuation," *IEEE Trans. Power Electron.*, vol. 33, no. 8, pp. 6595–6607, Aug. 2018.

[16] A. J. Korn, M. Winkelnkemper, and P. Steimer, "Low output frequency operation of the modular Multi-level converter," in *Proc. IEEE Energy Convers. Congr. Expo. Conf.*, Sep. 2010, pp. 3993–3997.

[17] L. He, K. Zhang, J. Xiong, S. Fan, and Y. Xue, "Low-Frequency ripple suppression for Medium-voltage drives using modular multilevel converter with full-bridge submodules," *IEEE J. Emerg. Sel. Top. Power Electron.*, vol. 4, no. 2, pp. 657–667, Jun. 2016.

[18] K. Wang, Y. Li, Z. Zheng, and L. Xu, "Voltage balancing and fluctuation-suppression methods of floating capacitors in a new modular multilevel converter," *IEEE Trans. Ind. Electron.*, vol. 60, no no. 5, pp. 1943–1954, May. 2013.

[19] M. Huang, J. Zou, X. Ma, Y. Li, and M. Han, "Modified modular multilevel converter to reduce submodule capacitor voltage ripples without Common-mode voltage injected," *IEEE Trans. Ind. Electron.*, vol. 66, no. 3, pp. 2236–2246, Mar. 2019.

[20] S. Du, B. Wu, N. R. Zargari, and Z. Cheng, "A Flying-capacitor modular multilevel converter for medium-voltage motor drive," *IEEE Trans. Power Electron.*, vol. 32, no. 3, pp. 2081–2089, Mar. 2017.

[21] R. Picas, J. Zaragoza, J. Pou, S. Ceballos, G. Konstantinou, and G. J. Capella, "Study and comparison of discontinuous modulation for modular multilevel converters in motor drive applications," *IEEE Trans. Ind. Electron.*, vol. 66, no. 3, pp. 2376–2386, Mar. 2019.

[22] R. Picas, S. Ceballos, J. Pou, J. Zaragoza, G. Konstantinou, and V. G. Agelidis, "Closed-Loop discontinuous modulation technique for capacitor voltage ripples and switching losses reduction in modular multilevel converters," *IEEE Trans. Power Electron.*, vol. 30, no. 9, pp. 4714–4725, Sep. 2015.

[23] K. Ilves, S. Norrga, L. Harnefors, and H.-P. Nee, "On energy storage requirements in modular multilevel converters," *IEEE Trans. Power Electron.*, vol. 29, no. 1, pp. 77–88, Jan. 2014.

[24] G. Guo *et al.*, "Application of third-order harmonic injection in a modular multilevel converter," *IEEE Trans. Ind. Electron.*, vol. 65, no. 7, pp. 5260–5271, Jul. 2018.

[25] C. Zhao, Z. Wang, Z. Li, P. Wang, and Y. Li, "Characteristics analysis of capacitor voltage ripples and dimensioning of full-bridge MMC with zero sequence voltage injection," *IEEE J. Emerg. Sel. Top. Power Electron.*, vol. 7, no. 3, pp. 2106–2115, Sep. 2019.

[26] C. Zhao *et al.*, "Energy storage requirements optimization of full-bridge MMC with third-order harmonic voltage injection," *IEEE Trans. Power Electron.*, vol. 34, no. 12, pp. 11661–11678, Dec. 2019.

[27] J. Wang, X. Han, H. Ma, and Z. Bai, "Analysis and injection control of circulating current for modular multilevel converters," *IEEE Trans. Ind. Electron.*, vol. 66, no. 3, pp. 2280–2290, Mar. 2019.

[28] L. Yang, Y. Li, Z. Li, P. Wang, S. Xu, and R. Guo, "Loss optimization of MMC by second-order harmonic circulating current injection," *IEEE Trans. Power Electron.*, vol. 33, no. 7, pp. 5739–5753, Jul. 2018.

Ming Huang was born in Shaanxi, China, in 1989. He received the B.S. degree from the Hefei University of Technology, Hefei, China, in 2011, and the Ph.D. degree from Xi'an Jiaotong University, Xi'an, China, in 2019, both in electrical engineering.

From 2017 to 2018, he was a Visiting Scholar with the Center for Ultra-Wide-Area Resilient Electric Energy Transmission Networks (CURENT), University of Tennessee, Knoxville, TN, USA. Since 2019, he has been a Faculty Member with the School of Automation form Northwestern Polytechnical University, Xi'an, China, where he is currently an Associate Professor.

His research interests include applications of modular multilevel converters, MVdc motor drive control, and dc transformers.

Zhen Kang (Member, IEEE) was born in Shanxi, China, in 1988. He received the B.S. and Ph.D. degrees in school of electrical engineering from Xi'an Jiaotong University, in 2010 and 2016, respectively.

From December 2016 to June 2017, he was an Engineer at the Jiangsu Electric Power Company Research Institute, Nanjing 210036, China. Since July 2017, he has been an Assistant Professor with the School of Automation, Northwestern Polytechnical University, Xi'an, China. His research interests include areas of developing the efficiency of the precise-integration time-domain method and numerical methods in solving electromagnetic problems, and applications of modular multilevel converters, MVdc motor drive control, and dc transformers.

Weilin Li (Member, IEEE) received the B.S. and M.S. degrees from the Northwestern Polytechnical University, Xi'an, China, in 2007 and 2009, respectively, and the Ph.D. degree from the Institute for Automation of Complex Power Systems, E.ON Energy Research Center, RWTH Aachen University, Aachen, Germany, all in electrical engineering.

He is currently with the Department of Electrical Engineering, Northwestern Polytechnical University, as a Full Professor. His research interests include integration of renewable generations, protection in medium voltage dc (MVdc) power system, and power electronic applications in smart grid. He has authored or coauthored for more than 50 peer-reviewed journals and conference papers.

Jianlong Zou was born in Shandong, P.R. China, in 1976. He received the B.Sc., M.Sc., and Ph.D. degrees in electrical engineering from Xi'an Jiaotong University, P.R. China, in 1999, 2002, and 2008, respectively.

In 2002, he joined the Faculty of Electrical Engineering, Xi'an Jiaotong University, where he is currently an Associate Professor. He also has good cooperation with The Hong Kong Polytechnic University. In 2012, he was a Visiting Scholar at the Michigan State University, Michigan, USA. His main areas of research interests include modular multilevel converter based HVdc, wind generation, and nonlinear dynamics in electrical engineering.

Xikui Ma was born in Shaanxi, China, in 1958. He received the B.Sc. and M.Sc. degrees in electrical engineering from Xi'an Jiaotong University, Xi'an, China, in 1982 and 1985, respectively.

In 1985, he joined as a Lecturer with the Faculty of Electrical Engineering, Xi'an Jiaotong University, where he became a Professor in 1992. During the academic year 1994–1995, he was a Visiting Scientist at the Department of Electrical Engineering and Computer, University of Toronto, ON, Canada. He is the author or co-author of more than 140 scientific and technical papers on these subjects, and also the author of five books in electromagnetic fields. His current research interests include electromagnetic field theory and its applications, analytical and numerical methods in solving electromagnetic problems, chaotic dynamics and its applications in power electronics, and the applications of digital control to power electronics.

Jianhua Li was born in Shaanxi, China, in 1987. He received the B.S. degree in automation from the Central South University, Changsha, China, in 2011, and the M.S. degree in electrical engineering from Xi'an Jiaotong University, Xi'an, China, in 2013.

Since 2013, he has been working with the State Grid Xian Electric Power Supply Company, Xi'an, Shaanxi, China, as an Engineer. His research interests include substation operation and maintenance, and the live detection of power equipment.